ISA Transactions xxx (xxxx) xxx

Contents lists available at ScienceDirect

ISA Transactions

journal homepage: www.elsevier.com/locate/isatrans

Research article

Control of a two-DOF parallel robot with unknown parameters using a novel robust adaptive approach

Saeed Ansari Rad [a], Mehran Ghafarian Tamizi [a], Amin Mirfakhar [b], Mehdi Tale Masouleh [a,*], Ahmad Kalhor [a]

[a] Human and Robotic Interaction Laboratory, School of Electrical and Computer Engineering, University of Tehran, Tehran, Iran
[b] University of Science and Technology, Tehran, Iran

ARTICLE INFO

Article history:
Received 27 April 2019
Received in revised form 4 January 2021
Accepted 2 February 2021
Available online xxxx

Keywords:
Robust adaptive control
2-DOF spherical parallel robot
Jacobian matrix
Simultaneous identification and control
Exponentially decay algorithm

ABSTRACT

Model-based methods lose their performance in confronting with model uncertainties and disturbances. Accordingly, some degrees of adaptation to the involved conditions are required. In this paper, a novel robust adaptive scheme is proposed which guarantees the simultaneous identification and control of a system in the presence of external disturbances. Thereafter, the suggested algorithm is implemented on a 2-DOf spherical parallel robot as a stabilizer device. By identifying unknown parameters of Jacobian matrix, the relative identification error is obtained as 0.0207. Applying external excitations to the base, the ratio of end-effector to base orientation is acquired as 0.091, demonstrating proper stabilization in comparison with other two well-known methods. The proposed structure also reveals a reliable performance in tracking desired paths for the end-effector Euler angles.

1. Introduction

One of the most important challenges in robotics consists in collecting information from an unknown environment which is carried out by installing different sensors. Inspired by human nature, the foremost way for obtaining information from the environment consists in capturing picture. In this regard, the camera can be regarded as one of the important installed component, i.e., sensor, of such robots. In order to obtain accurate information, the quality of image is of importance therefore image stabilization has become an integral part in different aspects of robotics such as humanoid, mobile robots and manipulators. The vision data in these systems can be interpreted as important as human eye data, 80 percent of which can be acquired from the environment [1].

Generally, there are four existing methods in stabilizing the image namely, mechanical, sensor-based, electronic, and digital approaches. The first technique adopts mechanical devices to keep the observable pathway of camera [2]. This methodology is mainly alluded to observable pathway adjustment and connected to image stabilization as well as other applications that require point based stabilization. In this kind, the greater part of stabilizer component is the gimbals structure with 2 or 3 axes [3]. The second method, commonly employed in commercial cameras, relies on controlling the image sensor or lens in order to keep the optical path continually at the same position on the image sensor [4,5]. The two final strategies are benefited from some properties which both manipulate the image itself to damp undesirable perturbation. The third one, regularly known as electronic image stabilization, utilizes incorporated inertial sensor [6]; however, the fourth technique, frequently regarded as digital image stabilization, employs the movement vector computed from feature matching or tracking algorithms [7,8].

For the purpose of this paper the first approach is adopted, where the camera is balanced by a 2-Degree-of-Freedom (DOF) Spherical Parallel Robot (SPR), namely TezGoz, which is designed in the Human and Robot Interaction Laboratory, University of Tehran for image stabilization purposes. In the literature, several methods are proposed in order to use a SPR as a camera stabilizer. In [9], an image based control architecture is developed for tracking an object with a 2-DOF SPR. Danaei et al. [10] presented a 2-DOF gimbal system for image stabilizing and developed two control algorithms, exponentially decay and sliding mode control. Moreover, in [11] dynamic analysis of a 2-DOF SPR is presented which adopted the computed torque method for tracking object. Safaryazdi et al. [12] proposed a real-time controller for a camera stabilizer utilizing a 2-DOF SPR by using multi-thread programming concept for displaying control results, simultaneously.

To the end of controlling a stabilizer, two structures can be employed. The first method is the direct method where a gyro

* Corresponding author.
E-mail addresses: Saeedansari71@ut.ac.ir (S. Ansari Rad), mehran.ghafarian@ut.ac.ir (M. Ghafarian Tamizi), mirfakhar_amin@mecheng.iust.ac.ir (A. Mirfakhar), m.t.masouleh@ut.ac.ir (M.T. Masouleh), akalhor@ut.ac.ir (A. Kalhor).

https://doi.org/10.1016/j.isatra.2021.02.001
0019-0578/

sensor is mounted on the gimbal End-Effector (EE), and the second one is the indirect strategy utilizing a gyro sensor mounted on the movable platform [13]. According to the foregoing methods, several control algorithms are presented in literature. In [14], a linear quadratic Gaussian with loop transfer recovery method is compared with a lead Proportional–Integral (PI) controller. Furthermore, in [15] nonlinear fuzzy PI controller is suggested in order to control a stabilizer. Zakia et al. [16] proposed a combination of sliding mode and traditional PID control scheme for a 2-DOF serial planar manipulator, and in [17] a vision-based method intended to position control of a 2-DOF serial planar robot manipulator is proposed. In [18], a robust controller is developed for a robot manipulator based on a self-tuning fuzzy PID and fast terminal sliding mode control. In [19], a robust controller is designed in order to improve the performance of a 2-DOF robotic arm under disturbance. Yin et al. [20] proposed an adaptive robust tracking control for trajectory tracking of a 6-DOF industrial robot in the presence of external disturbances. The research conducted in [21] is associated with a previous study on 2-DOF Agile Eye [11,22], intended to introduce an adaptive method in order to cope with uncertainty of the actuators while stabilization of the robot EE. As for providing data about the joint space and the desired Encoder position, the algorithm computes the Inverse Jacobian Matrix and uses the angular position of each encoder, which makes it dependent on the accuracy of Jacobian expressions and the system model which relates directly the performance of the robot to the accuracy of the two latter parameters. Thus, emerging here is the notation of model identification which is the main objective of this paper.

In general cases, robust adaptive control methods [23–27] have been much more employed recently due to their agility and robustness. Evolutionary approaches [28,29] have been recently introduced, as well. Nevertheless, in these model-based methods, the plant should be modeled comprehensively and most of the time, the analytical procedures represent a complicated and time-consuming process, in parallel robots in particular. Notwithstanding the fact that the simplified version of such models attempts to cope with complexities, it leads to reduce in the accuracy of control procedure. Moreover, the obtained model is not adaptable in the case of possible disturbance and uncertainties of practical implementation which are mainly arise from mechanical backlash and unreliability of mechanical construction. Accordingly, as a remedy to the latter limitations, an algorithm is required for identifying system properties and coping with varying surrounding environment. From a control standpoint, an especial designing method which simultaneously performs identification and control of the robot with unknown parameters seems a prerequisite and a definite asset in practice. There exists huge motivation toward intelligent strategy which avoids the complex mathematic calculations, in parallel robots in particular. This lays the groundwork for a new generation of automatic control strategies which seek simultaneously for less complex calculations and higher performance. It should be noted that resorting to intelligent approaches, i.e., learning-based algorithms to identify and control complex robotic mechanical systems, stimulated the interest of many researches involved in the foregoing topics [30,31].

One of the most important challenges in identifying the system unknown parameters is instability of the closed-loop process in the intended procedure. Most of proposed methods propounded in the literature are based on so-called Lyapunov theory in order to guarantee closed-loop stability. As a case, Xu et al. [32] suggested a method for continuous nonlinear systems during identification by using the latter theorem. Moreover, Jahandari et al. [33] suggested a procedure which includes a combination of the recursive least square and the Lyapunov theorem. In [34], recurrent fuzzy neural networks have been utilized for identification and control of non-linear dynamic systems. Ren et al. [35] suggested a dynamic neural network for control and identification of unknown Multi-Input/Multi-Output (MIMO) continuous-time non-linear systems. In [36], for MIMO non-linear systems with uncertainty and having non-symmetric input constrains, adaptive tracking control is designed in which states of auxiliary design system are used. By employing a recurrent fuzzy system, Dass et al. [37] presented a procedure for identification and control of non-linear dynamical systems. In [38], an improved PID controller as well as study on the parameters identification of hydraulic system is carried out. Predicated on the aforementioned researches, guaranteeing closed-loop stability while identification of parameters is another concern. Although in the corresponding literature researches provide a sufficient guarantee for control procedure, from the best knowledge of the authors, in the most cases it has been assumed that the identified parameters had already reached their true values. Owning to this fact, initial conditions and convergence of parameters play a critical role in the simultaneous identification and control scheme.

Another approach for identifying and controlling a system with unknown parameters consists in employing automatic control methods. In this regard, learning-based algorithms are utilized to acquire optimal policy. For instance, in [39], an integral Q-learning approach is proposed for Continuous-Time (CT) linear time-invariant systems in order to solve a Linear Quadratic Regression (LQR) problem without having prior-knowledge about the system dynamics. Yu Jiang et al. [40] suggested a novel policy iteration approach for obtaining on-line adaptive optimal controllers for CT linear systems with unknown dynamics. Modares et al. [41] developed an on-line learning algorithm in order to solve the LQR problem for partially-unknown CT systems. In [42], a combination of off-policy learning and experience-replay for output regulation tracking control of CT linear systems with completely unknown dynamics is presented. In [43], a learning algorithm is introduced in order to improve the capability of identification procedure which provides better adaptive capability to the change of the surrounding environment. Unfortunately, most of the proposed learning-based method offer complicated policies which demand lots of process, analysis, and in some cases huge amount of data samples. Furthermore, these policies are mostly designed for linear time-invariant systems, which reduces the performance of control method in the case of confronting with realistic conditions.

There are a few conducted researches trying to move toward intelligent control, that is to go beyond having actual system model. In [44], a scheme for impedance control of a robot manipulator has been developed by using the so-called Szasz–Mirakyan approximation for tuning coefficients of the adaptive laws in order to uncertainty compensation and enhancing the tracking error. Moreover, in [45] an adaptive robust control is proposed for the control of a 2-DOF lower limb robot system in which the first part tracks a desire path regardless of uncertainties and disturbances, and in the other part with a fuzzy set the gain of optimal design approach is determined. In [46], an adaptive robust control approach is proposed to achieve tracking control of an under-actuated quad-rotor regardless of initial constraint deviation and mismatched uncertainties. Nonetheless, all these researches have been carried out only to the numerical simulation extend so far. The mentioned idea is extended to the real-time case experiments, too. In [47], an adaptive robust integral sliding mode controller is proposed in order to enhance pitch angle control performances of a generator power fluctuations for wind turbines. In this regard, an adaptation law is synthesized to accurately track the desired trajectory and compensate for model uncertainties and uncertain disturbances. In [48], a fast terminal sliding mode control is proposed to regulate the position of a 4-DOF mobile lower limb exoskeleton assisting the sit-to-stand and

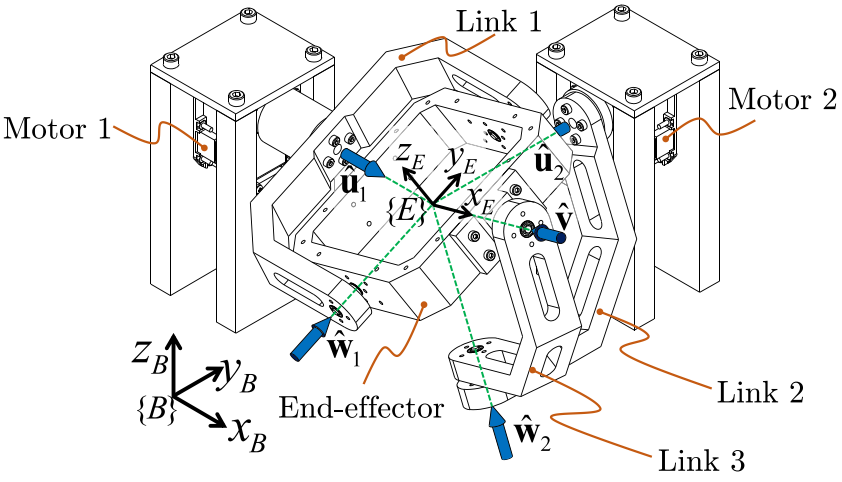

Fig. 1. Mechanical structure of the TezGoz a 2-DOF spherical parallel robot [10].

stand-to-sit tasks for elderly people. The method has succeeded in dealing with non-modeled dynamics, ensuring a rapid convergence, and reducing the chattering effect. The aforementioned applied systems suffer relatively with less complex dynamics in comparison to SPR. The applied adaptive methods do not provide any information on system behavior, they require partial system prior knowledge in the identification procedures, and are often limited to a specific system type or model.

To elude the aforementioned issues, in this paper a novel method has been introduced in order to stabilize a 2-DOF SPR. The main contribution of the paper can be classified into the following topics: (1) In order to adapt with varying conditions through the control procedure, a robust adaptive scheme has been proposed, to end of identifying the unknown system parameters and tracking the desired path for control purposes. By providing a strong guarantee in simultaneous identification of system parameters and system output control, the proposed method prevents the instability of closed-loop system. In another word, the mentioned problems in convergence and initial conditions of the identified parameters, as well as adaptation to uncertainties and environment variations, are solved by implementing the proposed scheme. (2) By avoiding from challenges of model-based approaches, the unknown parameters of an equivalent model are obtained without having any prior knowledge on traditional kinematics or dynamic calculations. Indeed, it will be shown that the identified adaptive model converges to the predominant behavior of the system in the steady state. Nonetheless, avoiding from designing complicated policies or heavy computational expenses, the proposed algorithm is applicable in the robotic field in which the aforementioned automatic algorithms encounter implementation difficulties.

The remainder of the paper can be organized as follows. Firstly, in order to provide a mathematic view from the Jacobian matrix of the 2-DOF SPR, in Section 2 the kinematic properties of the under study robot is briefly reviewed. It is vital to mention that the latter section is devoted to Jacobian matrix calculations to provide a verification for the results of the proposed method and also required information for the other two methods that have been employed in the paper as reference methods. In Section 3, the basic notion of the robust adaptive approach has been thoroughly explained. By proposing a time-varying model in the presence of bounded disturbances, one can guarantee the simultaneous identification and control of a system. In Section 4, the simulation results have been demonstrated which shows the superiority of the proposed novel method in comparison with the other well-known methods. Finally, in Section 5, the practical results of the 2-DOF SPR are provided, revealing practical verifications for the proposed method.

2. Kinematic analyses

In this section, required kinematic equations for verification of Jacobian matrix are obtained. Fig. 1 illustrates the schematic of 2-DOF SPR. In this robot, as depicted in Fig. 1, the EE is attached to the base by three identical kinematic limb structures in which all axes of the joints, including the actuators, pass through one point, called the writs point. Moreover, the axes of two consecutive joints are perpendicular to each other.

In parallel manipulators, the time rate changes of the EE pose, namely the twist of EE, $\boldsymbol{t}$ is mapped to the time rate changes of the joint space, $\dot{\boldsymbol{\theta}}$, through the Jacobian matrix, $\boldsymbol{J}$, as follows [49]:

$$\dot{\boldsymbol{\theta}} = \boldsymbol{J}\boldsymbol{t} \tag{1}$$

In the case of the under study parallel robot, $\boldsymbol{\theta}$ is the position vector of the first joint; i.e. the actuator, and the twist of the EE consists in only the angular velocity, $\boldsymbol{\omega}_e$, including ω_x, ω_y, and ω_z. From the study conducted in [50], for the Jacobian matrix of the 2-DOF SPR, one has:

$$\boldsymbol{J} = \begin{bmatrix} \frac{\hat{\mathbf{u}}_1^\top - \cos\alpha_1 \hat{\mathbf{w}}_1^\top}{\sin^2\alpha_1} \\ \frac{(\hat{\mathbf{v}}\times\hat{\mathbf{w}}_2)^\top}{(\hat{\mathbf{v}}\times\hat{\mathbf{w}}_2)^\top\hat{\mathbf{u}}_2} \end{bmatrix} \tag{2}$$

where

$$\begin{aligned} \hat{\mathbf{u}}_1 &= \begin{bmatrix} 1 & 0 & 0 \end{bmatrix}^\top \\ \hat{\mathbf{u}}_2 &= \begin{bmatrix} 0 & -1 & 0 \end{bmatrix}^\top \\ \hat{\mathbf{w}}_1 &= \begin{bmatrix} 0 & \cos\theta_1 & \sin\theta_1 \end{bmatrix}^\top \\ \hat{\mathbf{w}}_2 &= \begin{bmatrix} -\sin\theta_2 & 0 & \cos\theta_2 \end{bmatrix}^\top \\ \hat{\mathbf{v}} &= \frac{\begin{bmatrix} -\cos\theta_1\cos\theta_2 & \sin\theta_1\sin\theta_2 & -\cos\theta_1\sin\theta_2 \end{bmatrix}^\top}{\sqrt{1-\sin^2\theta_1\cos^2\theta_2}} \end{aligned} \tag{3}$$

Moreover, α_1, as a geometrical parameter, shown in Fig. 2, which is equal to $\pi/2$. By substituting Eq. (3) into Eq. (2), the Jacobian matrix is simplified to:

$$\boldsymbol{J} = \begin{bmatrix} 1 & 0 & 0 \\ -\tan\theta_1\cos\theta_2\sin\theta_2 & -1 & -\tan\theta_1\sin^2\theta_2 \end{bmatrix} \tag{4}$$

where θ_1 and θ_2 is the position of actuators 1 and 2, respectively.

3. Online identification of Jacobian matrix and stabilization of 2-DOF SPR via a robust adaptive scheme

In this section, the robust adaptive scheme [51] is explained by taking into account the presence of bounded disturbances.

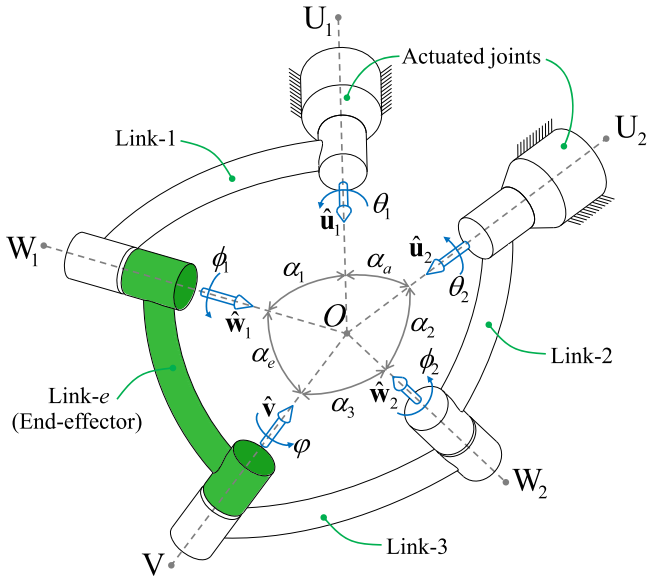

Fig. 2. Structure of 2-DOF SPR [50].

Thereafter, by demonstrating the fact that the steady state value of the identified transfer function bears resemblance to the order-reduced version of Jacobian matrix, the simultaneous identification and control of 2-DOF SPR becomes possible.

The basic model of a MIMO system is considered as:

$$\boldsymbol{G}(S) = \begin{bmatrix} \frac{b_{11}}{S-a_1} & \frac{b_{12}}{S-a_1} \\ \frac{b_{21}}{S-a_2} & \frac{b_{22}}{S-a_2} \end{bmatrix} \tag{5}$$

where the Laplace variable is shown with symbol S. Each output channel differential equation can be written as:

$$\dot{y}_q = a_q y_q + \boldsymbol{b}_q^\top \boldsymbol{u} + d_q = \boldsymbol{\varphi}_q^\top \boldsymbol{\Phi}_q + d_q;\ \forall q = 1, 2 \tag{6}$$

where d_q is a bounded disturbance in qth channel, whose upper bound is considered as $\bar{d}_q$. Moreover, for each channel, vectors of nominator coefficients, system parameters, and channel regressors are calculated as follows:

$$\boldsymbol{b}_q^\top = [b_{q1}, b_{q2}],\ \ \mathbf{B} = \begin{bmatrix} \boldsymbol{b}_1^\top \\ \boldsymbol{b}_2^\top \end{bmatrix}$$

$$\boldsymbol{\varphi}_q^\top \in \mathbb{R}^{1\times 3} = [a_q, \mathbf{b}_q^\top],\ \ \boldsymbol{\Phi}_q \in \mathbb{R}^{3\times 1} = \begin{bmatrix} y_q \\ \boldsymbol{u} \end{bmatrix} \tag{7}$$

Assumption I. The matrix $\mathbf{B}$ is assumed to be diagonally dominant in which both conditions $|b_{11}| > |b_{12}|$ and $|b_{22}| > |b_{21}|$ are established.

Sliding rules force the system to gain our target features by sliding along a cross-section of the system's normal behavior. In order to track output signals and reduce output error, sliding rules at each channel are defined:

$$s_q = \widetilde{y}_q = y_q - y_{r_q};\ \forall q = 1, 2 \tag{8}$$

where, s_q denotes the sliding variable in each channel. Desired signals, y_{r_q}, are continuous and considerably smooth. Accordingly, the control input vector, $\widehat{\mathbf{u}}$, is calculated, which forces the system to reach sliding surfaces. Moreover, the vector of input signals is applied to the system plant based on the following expression:

$$\boldsymbol{u} = \hat{\boldsymbol{u}} - \boldsymbol{\eta}\,\mathrm{sign}(\boldsymbol{S}) \tag{9}$$

where,

$$\hat{\boldsymbol{u}} = \widehat{\mathbf{B}}^{-1}\left(\begin{bmatrix} \dot{y}_{r_1} \\ \dot{y}_{r_2} \end{bmatrix} - \begin{bmatrix} \widehat{a}_1 y_1 \\ \widehat{a}_2 y_2 \end{bmatrix}\right),\ \boldsymbol{\eta} = \mathrm{diag}\,(\eta_1, \eta_2)\,,\ \boldsymbol{S} = \begin{bmatrix} s_1 \\ s_2 \end{bmatrix}. \tag{10}$$

Remark 1. The sign of elements of $\boldsymbol{\eta}$ is determined such that $\eta_1 b_{11} > 0$ and $\eta_2 b_{22} > 0$. Furthermore, the suitable value of each element should be chosen such that both $|\eta_1| > \frac{\bar{d}_1}{|b_{11}|-|b_{12}|}$ and $|\eta_2| > \frac{\bar{d}_2}{|b_{22}|-|b_{21}|}$ are yielded.

The hat mark ($\widehat{\ }$) on each parameter shows the estimated value of that parameter. Likewise, the tilde mark ($\widetilde{\ }$) on each parameter stands for the difference value of such parameter from its real value.

$$\dot{\boldsymbol{S}} = -\widetilde{\mathbf{B}}\,\hat{\boldsymbol{u}} + \begin{bmatrix} \widetilde{a}_1 \widetilde{y}_1 \\ \widetilde{a}_2 \widetilde{y}_2 \end{bmatrix} - \mathbf{B}\boldsymbol{\eta}\,\mathrm{sign}(\boldsymbol{S}) + \mathbf{d} \tag{11}$$

where, $\mathbf{d} = \begin{bmatrix} d_1 & d_2 \end{bmatrix}^\top$ is the output disturbance vector. The error equation for each output channel is calculated as Eq. (12), where $\widetilde{\boldsymbol{\varphi}}_q \in \mathbb{R}^{3\times 1}$ denotes the identification error of system parameters:

$$e_q = \dot{y}_{r_q} - \dot{y}_q = \widetilde{\boldsymbol{\varphi}}_q^\top \boldsymbol{\Phi}_q + d_q;\ \forall q = 1, 2 \tag{12}$$

The symmetric covariance matrix of each channel regressors is calculated as follows:

$$\dot{\mathbf{R}}_q = -\alpha_q \mathbf{R}_q + \boldsymbol{\Phi}_q \boldsymbol{\Phi}_q^\top;\ \forall q = 1, 2 \tag{13}$$

where α_q denotes forgetting factor of qth channel. By applying sufficient excitation for both channels, the following inequalities are established:

$$\forall t > 0, \forall q = 1, 2 : 0 < \underline{\sigma}_q \mathbf{I}_3 \le \mathbf{R}_q(t) \le \bar{\sigma}_q \mathbf{I}_3 \tag{14}$$

where, $\underline{\sigma}\sigma_q$ and $\bar{\sigma}_q$ are the smallest and largest singular values of $\mathbf{R}_q$.

Suggested adaptation rules for model parameters are represented as follows:

$$\dot{\widehat{\boldsymbol{\varphi}}}_q = \mathbf{R}_q^{-1}\Big(\boldsymbol{\Phi}_q e_q + \underbrace{\begin{bmatrix} y_q \\ -\hat{\boldsymbol{u}} \end{bmatrix}}_{\boldsymbol{\phi}_q} s_q\Big);\ \forall q = 1, 2 \tag{15}$$

The first part in the right side bears resemblance to the continuous-time RLS updating rule. The second one is concerned with adaptive changes based on sliding values. After reaching sliding surfaces, this part is eliminated and only the first one affects adaptation rules.

In [29], it has been shown that the proposed robust adaptive controller is applicable in the case of dealing with linear time-invariant systems in absence of any disturbances, where the convergence of system parameters to their exact values is guaranteed—as well as the tracking of output signals. Hereafter, in the presence of bounded disturbances, the required theorem and the corresponding proof are presented as follows.

Definition 1. Persistent Excitation (PE) [52]: The bounded vector signal $\boldsymbol{z}(t)$ is PE over the interval $[t, t+T_1]$ if there exists $T_1 > 0$, $\gamma_1 > 0$, and $\gamma_2 > 0$, such that for all t:

$$0 < \gamma_1 \boldsymbol{I} \le \int_t^{t+T_1} \boldsymbol{z}(\tau)\boldsymbol{z}^\top(\tau)d\tau \le \gamma_2 \boldsymbol{I} \tag{16}$$

Remark 2. Predicated on Definition 1, in the RLS-based methods, model parameters are traceable if regressors are at least persistent excited with order of the number of parameters that are required to be estimated [52]. In this regard, one can assert, if each desired signal is at least PE with order 1, then model parameters are traceable and the corresponding covariance matrix

always remains positive definite. On the other hand, a desired signal with the order less than 1 in a channel is considered as an insufficient excitation for the channel.

In Theorem 1, it has been assumed that both output channels enjoy the PE desired signals. The case of insufficient excitation for the proposed method is completely surveyed in [29], in which by employing an evolving linear model, the problem for simultaneous identification and control is handled. In Procedure 1, the abstract of the proposed robust adaptive structure as well as the solution for insufficient excitation based on the order-reduced models is introduced.

Theorem 1. *For the considered system presented by Eq. (5) with sufficient excitation condition and an error upper bound as* $\bar{\boldsymbol{d}} = [\bar{d}_q]_{2\times 1}$, *and keeping with Assumption I and Remark 1, the identified parameters are guaranteed to converge to the vicinity of their exact values:*

$$\|\widetilde{\boldsymbol{\varphi}}(t\to\infty)\| \le \|\widetilde{\boldsymbol{\varphi}}\|_{\text{dist}}^{\max} \tag{17}$$

where

$$\widetilde{\boldsymbol{\varphi}}^{\top} = [\,\widetilde{\boldsymbol{\varphi}}_1^{\top}, \widetilde{\boldsymbol{\varphi}}_2^{\top}].$$

Furthermore, tracking errors of the desired output signals are guaranteed to be bounded; the upper bounds are formulated as follows:

$$\underset{t\to\infty}{|\tilde{y}_q(t)|} \le \bar{c}_{dist}^{\,q} \tag{18}$$

where

$$\bar{c}_{dist}^{\,q} = \|\widetilde{\boldsymbol{\varphi}}\|_{\text{dist}}^{\max}\sqrt{2\underline{\sigma}};\ \ 0<\underline{\sigma}=\min\{\underline{\sigma}_1,\underline{\sigma}_2\}$$

and the closed-loop system stays stable.

Proof. Consider the following Lyapunov function:

$$V = \frac{1}{2}\left(\boldsymbol{S}^{\top}\boldsymbol{S} + \sum_{q=1}^{2}\widetilde{\boldsymbol{\varphi}}_q^{\top}\mathbf{R}_q\,\widetilde{\boldsymbol{\varphi}}_q\right). \tag{19}$$

Substituting the value of control inputs from Eq. (10) into Eq. (11), one can write:

$$\dot{\boldsymbol{S}} = -\widehat{\mathbf{B}}\widehat{\mathbf{B}}^{-1}\left(\begin{bmatrix}\dot{y}_{r_1}\\ \dot{y}_{r_2}\end{bmatrix} - \begin{bmatrix}\widehat{a}_1 y_1\\ \widehat{a}_2 y_2\end{bmatrix}\right) + \begin{bmatrix}\widehat{a}_1\tilde{y}_1\\ \widehat{a}_2\tilde{y}_2\end{bmatrix} - \mathbf{B}\boldsymbol{\eta}\,\text{sign}(\boldsymbol{S}) + \mathbf{d}. \tag{20}$$

Substituting the derivative of sliding vector with respect to the time from Eq. (20) and performing some calculations, the derivation of the Lyapunov function is calculated as:

$$\dot{V} = \sum_{q=1}^{2}\left(s_q\begin{bmatrix}y_q & -\hat{\boldsymbol{u}}^{\top}\end{bmatrix} - \begin{bmatrix}\widehat{\boldsymbol{a}}_q^{\top} & \widehat{\boldsymbol{b}}_q^{\top}\end{bmatrix}\mathbf{R}_q\right)\widetilde{\boldsymbol{\varphi}}_q + \frac{1}{2}\sum_{q=1}^{2}\widetilde{\boldsymbol{\varphi}}_q^{\top}\dot{\mathbf{R}}_q\widetilde{\boldsymbol{\varphi}}_q$$
$$+ \sum_{q=1}^{2}s_q d_q - \sum_{q=1}^{2}\left(\eta_q\sum_{j=1}^{2}b_{qj}s_q\,\text{sign}\left(s_j\right)\right). \tag{21}$$

Based on the lower bound of $|\eta_q|$ in Remark 1 and according to Assumption I, the following inequality, is driven:

$$\dot{V} \le -\sum_{q=1}^{2}\left(\frac{1}{2}\alpha_q\widetilde{\boldsymbol{\varphi}}_q^{\top}\mathbf{R}_q\widetilde{\boldsymbol{\theta}}_q + \boldsymbol{\Phi}_q^{\top}\widetilde{\boldsymbol{\varphi}}_q\,d_q\right)$$
$$-\frac{1}{2}\sum_{q=1}^{2}\widetilde{\boldsymbol{\varphi}}_q^{\top}\,\boldsymbol{\Phi}_q\,\boldsymbol{\Phi}_q^{\top}\widetilde{\boldsymbol{\varphi}}_q - \sum_{q=1}^{2}\left|\eta_q\right|\left|b_{qq}\right|\left|s_q\right|. \tag{22}$$

Considering

$$|\,\boldsymbol{\Phi}_q^{\top}(t)\,\widetilde{\boldsymbol{\theta}}_q(t)\,d_q| < \frac{1}{2}|\alpha_q\widetilde{\boldsymbol{\theta}}_q^{\top}(t)\,\mathbf{R}_q(t)\,\widetilde{\boldsymbol{\theta}}_q(t)\,| \tag{23}$$

as the sufficient condition for each output channel, it can be written:

$$\dot{V} < -\frac{1}{2}\sum_{q=1}^{2}\widetilde{\boldsymbol{\varphi}}_q^{\top}\,\boldsymbol{\Phi}_q\,\boldsymbol{\Phi}_q^{\top}\,\widetilde{\boldsymbol{\varphi}}_q - \sum_{q=1}^{2}\left|\eta_q\right|\left|b_{qq}\right|\left|s_q\right|. \tag{24}$$

By applying the sufficient conditions from Eq. (23), one can conclude:

$$\dot{V} < -W_1(\|\boldsymbol{S}\|, \|\widetilde{\boldsymbol{\varphi}}\|) = -\frac{1}{2}\underline{\sigma}\,\|\widetilde{\boldsymbol{\varphi}}\|^2 - \delta\,\|\boldsymbol{S}\| < 0 \tag{25}$$

where

$$0 < \delta = \min_{\forall q=1,2}|\eta_q||b_{qq}|.$$

Therefore, based on the Lyapunov theory, the intended closed-loop system is guaranteed to be stable. The Lyapunov function, defined in Eq. (19), consists in two parts, the first expression shows the identification error level while the second part is devoted to the tracking error level. In this regard, guaranteeing convergence of the Lyapunov function to lower levels, both identification and tracking properties of the controller are guaranteed at the same time. Based on the sufficient conditions acquired in Eq. (23), one can calculate the following domain:

$$\bar{D}_1 = \Bigg\{\forall\widetilde{\boldsymbol{\varphi}}|, \widetilde{\boldsymbol{\varphi}}\in\mathbb{R}^{6\times 1}, \|\widetilde{\boldsymbol{\varphi}}\| \ge \underbrace{\max_{q=1,2}\left(\frac{2\,\bar{d}_q\max_t\left\|\boldsymbol{\Phi}_q(t)\right\|}{\alpha_q\underline{\sigma}_q}\right)}_{\|\widetilde{\boldsymbol{\varphi}}\|_{\text{dist}}^{\max}}\Bigg\}. \tag{26}$$

In fact, $\bar{D}_1$ determines the area where $\dot{V} < 0$. Therefore, the identification error will decrease in order that $\|\widetilde{\boldsymbol{\varphi}}\| \le \|\widetilde{\boldsymbol{\varphi}}\|_{\text{dist}}^{\max}$. If V^* represents the aforementioned domain, then one can infer that $\exists t_1 < \infty, \forall t > t_1 : V \le V^*$. Therefore, the following equation is calculated:

$$V^* = \frac{1}{2}\left\|\boldsymbol{S}^*\right\|^2 = V_{\min} = \underline{\sigma}\left(\|\widetilde{\boldsymbol{\varphi}}\|_{\text{dist}}^{\max}\right)^2. \tag{27}$$

where $\left\|\boldsymbol{S}^*\right\|$ is defined as $\forall t > t_1 : \|\boldsymbol{S}\| \le \left\|\boldsymbol{S}^*\right\|$. Based on the Final Value theorem and by employing Eq. (8), the following equations are obtained:

$$\forall q = 1,2 : \underset{t\to\infty}{|\tilde{y}_q|} = \underset{t\to\infty}{|s_q|}. \tag{28}$$

Considering the worst case in each channel, $|s_q| \le \left\|\boldsymbol{S}^*\right\|$, the following upper bound is calculated for the output signals:

$$\forall q = 1,2 : \underset{t\to\infty}{|\tilde{y}_q|} \le \underbrace{\sqrt{2\underline{\sigma}}\,\|\widetilde{\boldsymbol{\varphi}}\|_{\text{dist}}^{\max}}_{\bar{c}_{\text{dist}}^{\,q}}. \quad \square \tag{29}$$

Remark 3. In the proof of Theorem 1, the identification of the transfer function parameters and the closed-loop stability are guaranteed by exploiting sign($\boldsymbol{S}$) in Eq. (9). Nevertheless, as mentioned in Procedure 1, $\boldsymbol{\zeta}\tanh(\boldsymbol{\beta S})$, the smoother equivalent, is substituted in Eq. (9) in order to avoid chattering in the input signals.

Theorem 2. *For the described system by Eq. (5) with sufficient excitation condition, applying* $\boldsymbol{u} = \hat{\boldsymbol{u}} - \boldsymbol{\eta}\,\boldsymbol{\zeta}\tanh(\boldsymbol{\beta S})$ *as the system input vector, and keeping with Remark 1, the identified parameters are guaranteed to converge to the vicinity of their exact values:*

$$\|\widetilde{\boldsymbol{\varphi}}(t\to\infty)\| \le \|\widetilde{\boldsymbol{\varphi}}\|_{\text{chat}}^{\max} \tag{30}$$

Procedure 1 Robust Adaptive Scheme for evolving model

Initialization: $\forall q = 1, 2 : \widehat{a}_q(0) = 0, \widehat{\mathbf{B}}(0) = \mathbf{I}_2, \mathbf{R}_q(0) = 0.01 \times \mathbf{I}_3$
while $t < t_f$ **do**
  Calculate desired paths.
  $\forall q = 1, 2 : \boldsymbol{\Phi}_q = \begin{bmatrix} y_q \\ \boldsymbol{u} \end{bmatrix}$.
  $\forall q = 1, 2 : s_q = \widetilde{y}_q$
  $\boldsymbol{u} = \hat{\boldsymbol{u}} - \boldsymbol{\eta}\, \boldsymbol{\zeta} \tanh(\boldsymbol{\beta S}), \boldsymbol{\zeta} = \mathrm{diag}(\zeta_1, \zeta_2), \boldsymbol{\beta} = \mathrm{diag}(\beta_1, \beta_2)$.
  for $q = 1, 2$ **do**
    $e_q = \dot{y}_{r_q} - \dot{y}_q$
    $\dot{\mathbf{R}}_q(t) = -\alpha_q \mathbf{R}_q(t) + \boldsymbol{\Phi}_q \boldsymbol{\Phi}_q^{\top}$
    $\mathbf{R}_q(t + dt) = \mathbf{R}_q(t) + \dot{\mathbf{R}}_q(t)dt$
    Insufficient Excitation Detection: Calculate the nullity of $\mathbf{R}_q(t)$, n_q.
    if $n_q = 0$ **then**
      $\widehat{\boldsymbol{\varphi}}_q(t) = \mathbf{R}_q^{-1}(t)(\boldsymbol{\Phi}_q e_q + \boldsymbol{\phi}_q s_q)$
      $\widehat{\boldsymbol{\varphi}}_q(t + dt) = \widehat{\boldsymbol{\varphi}}_q(t) + \dot{\widehat{\boldsymbol{\varphi}}}_q(t)dt$
    else (Applying order-reduced models)
      Form $\mathbf{R}_q^{\prime -1}$ by Removing first row and column.
      $\dot{\widehat{\mathbf{b}}}_q(t) = \mathbf{R}_q^{\prime -1}\left(\boldsymbol{u}\, e_q - \hat{\boldsymbol{u}}\, s_q\right)$
      $\widehat{\mathbf{b}}_q(t + dt) = \widehat{\mathbf{b}}_q(t) + \dot{\widehat{\mathbf{b}}}_q(t)dt$
    end if
  end for
  put $t = t + dt$
end while

where

$$\|\widetilde{\boldsymbol{\varphi}}\|_{\mathrm{chat}}^{\max} = \frac{2\phi}{\beta^* \sqrt{\underline{\sigma}}}, \beta^* = \min_{q=1,2} \beta_q$$

Moreover, tracking errors of the desired output signals are guaranteed to be bounded:

$$\lim_{t \to \infty} |\tilde{y}_q(t)| \leq \bar{\mathcal{C}}_{chat}^{q} \tag{31}$$

where

$$\bar{\mathcal{C}}_{chat}^{q} = \|\widetilde{\boldsymbol{\varphi}}\|_{\mathrm{chat}}^{\max} \sqrt{\underline{\sigma}}$$

and the closed-loop system stays stable.

It is worth mentioning, one can provide a similar proof for this case; however, with slight changes, it leads to similar results, as well. In this regard, in Theorem 2, ζ_q, β_q are chosen such that the following inequalities hold:

$$\left|b_{qq}\right| > \sum_{j \neq q} r_{qj}^* \left|b_{qj}\right|, \quad q, j = 1, 2 \tag{32}$$

in which

$$\forall q \neq j, r_{qj}^* = \frac{\zeta_j}{\zeta_q \tanh\left(\beta_q S_q^*\right)} \tag{33}$$

and S_q^* is defined such that $\forall t : S_q \leq S_q^*$.

Moreover, ϕ is selected in such a way that the inequality $\zeta_q > (\tanh(\phi))^{-1}$ holds for both $q = 1, 2$. By so doing, $\bar{D}_2$ determines the area where derivation of the Lyapunov function, represented by Eq. (19), remains negative definite, i.e. $\dot{V} < 0$.

$$\bar{D}_2 = \left\{ \forall \boldsymbol{S}(t) \mid \boldsymbol{S}(t) \in \mathbb{R}^2, \|\boldsymbol{S}(t)\| \geq \frac{2\,\phi}{\beta^*} \right\} \tag{34}$$

The order-reduced form of Jacobian matrix for 2-DOF robot can be formulated as follows:

$$\begin{bmatrix} \dot{\theta}_1 \\ \dot{\theta}_2 \end{bmatrix} = \boldsymbol{J}_{\mathrm{red}}(\theta_1, \theta_2) \begin{bmatrix} \omega_1 \\ \omega_2 \end{bmatrix} \tag{35}$$

where, ω_1 and ω_2 are the value of the EE angular velocity relative to the ground frame described in the {E} coordinates (Fig. 1) for the x and y axes, respectively. Therefore, $\boldsymbol{J}_{\mathrm{red}}$ attributes 2 elements of EE angular velocity to the encoder velocities, $\dot{\theta}_1$ and $\dot{\theta}_2$, while the effect of third element of EE, which is indeed along the z axis of the {E} frame, on the encoder velocities is considered as bounded disturbance in each channel.

Considering Eq. (5), $\dot{\theta}_1, \dot{\theta}_2$ can be chosen as the input signals and similarly, α, β (the EE Euler angles along the x and y axes) stand for the system output signals. Consequently, based on the definition given in Eq. (35), one can assert that the final value of the transfer function leads to similar value of the inverse of order-reduced Jacobian matrix:

$$\boldsymbol{J}_{\mathrm{red}}^{-1}(\theta_1^*, \theta_2^*) = S\{\frac{1}{S}\boldsymbol{G}(S)\}_{S \to 0} = -\begin{bmatrix} \frac{b_{11}}{a_1} & \frac{b_{12}}{a_1} \\ \frac{b_{21}}{a_2} & \frac{b_{22}}{a_2} \end{bmatrix} \tag{36}$$

where, θ_q^* indicates the encoder position of qth motor at the stabilized state of the robot EE.

Remark 4. In Assumption I, it has been assumed that the matrix of nominator coefficients, **B**, is a diagonally dominant matrix. In this regard, a fully decouple restriction is not imposed to the system, only a relatively mild one is chosen in such a way that guarantees the asymptotic stability of the closed-loop system. In the previous versions of the robust adaptive approach, introduced in [29,51], similar assumption is adopted. In both simulation and practical results, it is demonstrated that the identified matrix of dominator coefficients is obtained in the similar form, that is, a diagonally dominant matrix. More precisely, in the 2-DOF spherical parallel robot **B** represents a diagonally dominant matrix in which both $|b_{11}| > |b_{12}|$ and $|b_{22}| > |b_{21}|$ are established.

By expanding on the Lagrangian behavior of parallel robots, there exist several researches including [53–55] in which the Lagrangian behavior of the studied cases is diagonally dominant, as well. Having this in mind, in the presented paper, it has been shown that the identified nominator matrix is mainly responsible for demonstrating the behavior of reduced-order Jacobian

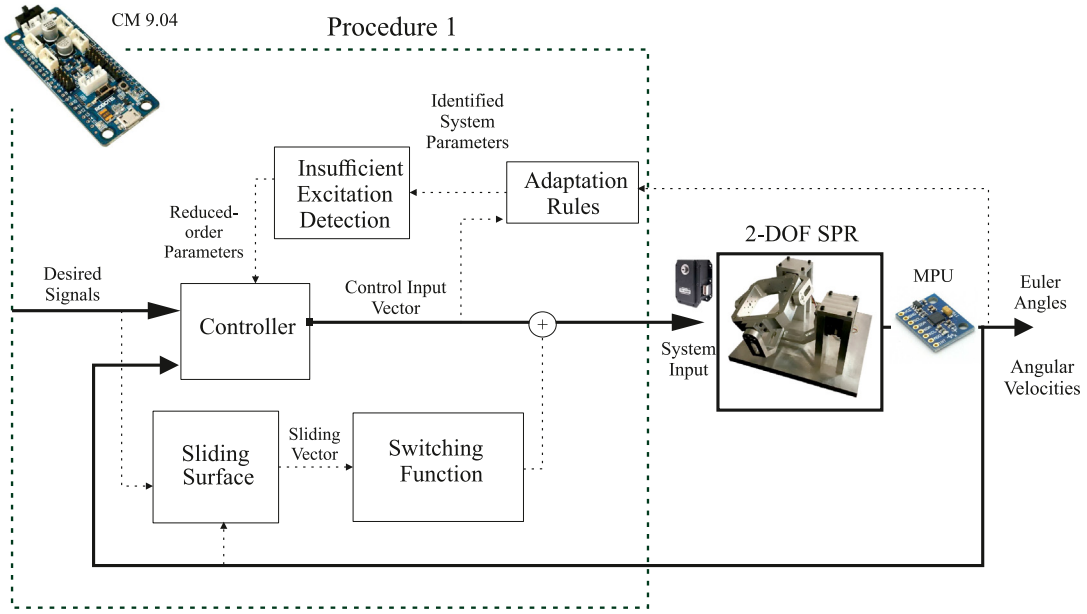

Fig. 3. The identification procedure.

matrix. One can deduce that the behavior of reduced-order Jacobian matrix in the stabilized state should bear resemblance to a diagonally dominant matrix, which is verified according to Eq. (4).

The major theoretical results of the paper falls into three parts: Firstly, in Theorem 1, it has been proven that the simultaneous identification and control of MIMO system in presence of bounded disturbances is guaranteed. In this regard, the effect of initial condition of identified parameters and their convergence rate on the stability of the closed-loop system has been reduced. Therefore, in the practical implementation, the stabilization of 2-DOF SPR has been guaranteed during the identification of its corresponding unknown parameters. This provides much better adaptability to the surrounding environment and disturbances in comparison to the model-based approaches. Secondly, it has been shown that the unknown system parameters are relevant to the elements of the reduced-order Jacobian matrix. In comparison to the other automatic control approaches, this provides much more conformity to the uncertainty and more importantly, brings about the least possible computational cost which makes it possible to be implemented on the practical MIMO plants. Thirdly, the number of identified parameters in the proposed version of robust adaptive approach is more than the other adaptive method such as [21], which provides better adaptability to the varying environment. Nonetheless, the possibility of occurrence of insufficient excitation pales since Procedure 1 handles the unbounded condition numbers via employing an evolutionary approach.

From Eq. (36), it can be inferred that in the steady state, only 4 independent parameters are enough for identifying the order-reduced Jacobian matrix, which is also revealed in some other researches, such as [21]. Nonetheless, by increasing the order of each channel, the proposed method employs two more parameters in the identification procedure. As shown in Procedure 1, whenever insufficient excitation occurs, the controller stops to update of a_q and attempts to estimate recursively the remaining 4 parameters in order to conform to the varying conditions.

Meanwhile, such a novel feature enables the controller to accomplish successfully control targets, among which, especially the smoothness of control input signals and stabilizing the external excitations, in the transient states. As thoroughly observed in Sections 4 and 5, the mentioned idea results in better performance in compare with implemented algorithms with classical approaches. Furthermore, the proposed robust adaptive approach guarantees the stability of the whole procedure and tracking the desired values. Thus, with the simultaneous identification and control of the transfer function of $\boldsymbol{G}(S)$, through the proposed method, one can obtain an order-reduced Jacobian matrix. Meantime, the control method tracks successfully the desired values of EE orientation without any prior knowledge.

In Fig. 3, the relationship between various parts of the identification procedure is depicted. In this regard, the information is measured from a gyro sensor, which comprises Euler angles and angular velocities, and is transferred to the controller. In this block, which represents the whole process of Procedure 1, the measured data as well as the control input is employed by adaptation rules in order to update the identified system parameters. In the next step, the degree of excitation is checked in order to regulate the condition number of covariance matrix Eq. (13) in each output channel. In the case of a correlated relation between the regressors, upon considering the reduced-order evolving models which are introduced in the Procedure 1, the reduced-order parameters are acquired in order to eliminate those correlated equations. Furthermore, the controller adopts the desired signal values, which in the condition of stabilization are obtained in such a way that the Euler angles and the angular velocities diminish, and the output of the MPU signals. The control input vector is calculated based on these values in order to convey the system through the specified path by the sliding surface. The system inputs, which are applied to the actuators in the velocity mode, adopts the control input vectors and the switching values of the sliding surfaces.

4. Simulation results

In this section, various aspects of the proposed structure for the simultaneous identification and control of the 2-DOF SPR are discussed through SimScape simulations. Firstly, by employing appropriate indices, the superiority of the proposed method is demonstrated over other well-known control methods. Thereafter, by determining desired paths for output signals, the performance of the proposed method in path tracking, which is crucial topic in object tracking, is shown, as well.

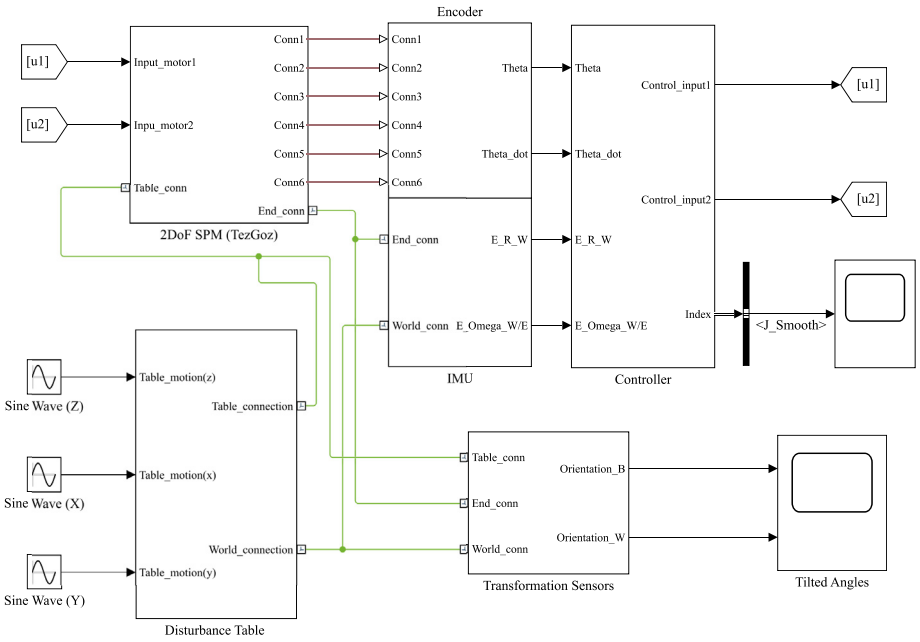

(a) SimMechanics block diagram of both Exponentially Decay and the adaptive algorithms

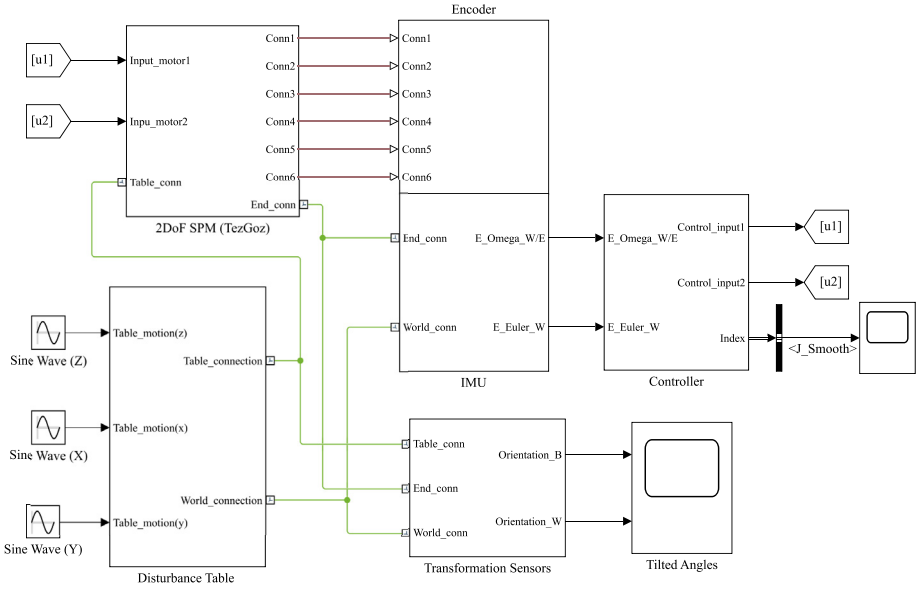

(b) SimMechanics block diagram of the proposed method

Fig. 4. Comparing between the structure of the proposed method and the previous implemented methods.

4.1. Online identification and stabilization

In this part, the details of the proposed method are thoroughly discussed via different simulations. The SimMechanics model of the proposed method, partly observed in Fig. 4, is developed by MATLAB software. In this regard, several blocks are employed to visualize the function of each part, among which, the controller block plays an important role to provide vivid view on the interaction between the proposed method and the plant. Moreover, other elements including IMU, Transformation Sensors, and Disturbance Table are shown in the SimMechanics block diagram. In the following simulation studies, by applying sinusoidal excitations to the disturbance table, coordinates of the base axes rapidly change. Sinusoidal signals excite different modes of the plants and are the best candidate for the identification purpose. In order to evaluate the performance of the proposed algorithm in the realistic conditions, different uncertainty and errors, gyro

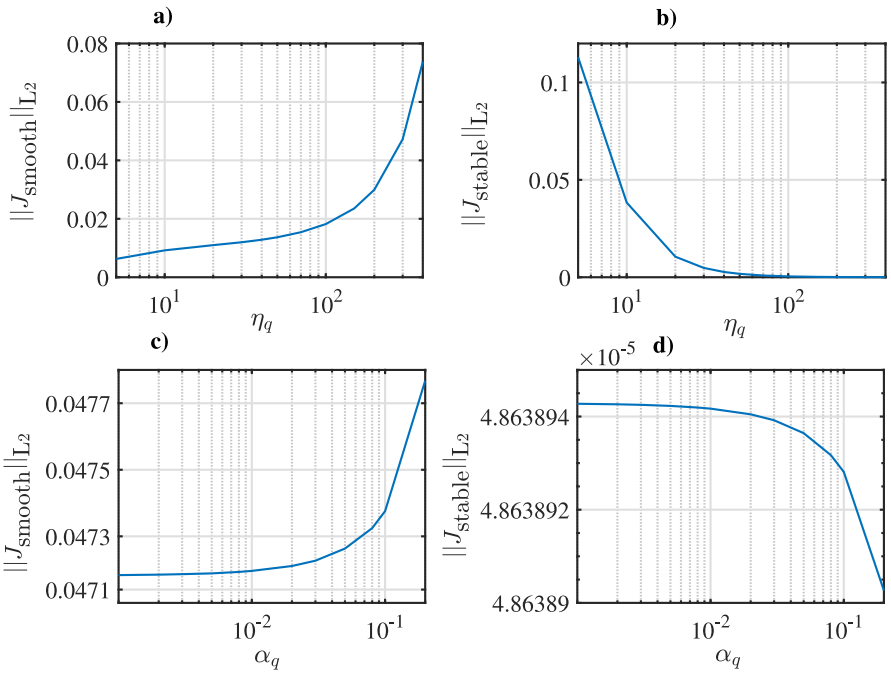

Fig. 5. The simulation results of the proposed scheme: Demonstrating the effect of η_q on the L_2-norm of (a) J_{smooth} and (b) J_{stable} and (c), (d) the effect of α_q on the mentioned indices.

noises, and external disturbances are considered in the simulation studies.

The model uncertainty in actuator parameters is shown by x_{dist}, which in the following simulations is set as constant value 0.5°. Moreover, noise in the gyro signals, modeled with white banded noise with power of 0.01, is denoted by x_{noise}. Another side of realistic conditions is devoted to the control input saturation. Bearing in mind that Dynamixel MX-64 is used in the implementation phase of 2-DOF SPR, 2 (rad/s) is chosen for each actuator saturation in the robot model. External excitations, applied to the base of the robot, are perfect tool for analyzing a stabilizing algorithm. In this regard, the harmonic around each axis is selected as:

$$\theta_{\text{exc}_j} = a_j \sin(f_j t), \quad j = x, y, z \tag{37}$$

where the amplitude of base excitation signals are set to $a_x = 0.3$ (rad), $a_y = 0.3$ (rad), and $a_z = 0.1$ (rad). Moreover, the corresponding frequencies are set to $f_x = 4$ (rad/s), $f_y = 2$ (rad/s), and $f_z = 1.24$ (rad/s). Such harsh excitations impose difficult conditions to the stabilizer, provide the opportunity to bring varied stabilizers into challenge and to find the most appropriate one.

In the following simulations, two important indices are determined for quantitative analysis. The first one, J_{stable}, is utilized to measure the norm of difference between orientation of EE toward the world frame and the corresponding desired vector:

$$J_{\text{stable}} = \left\| {}^{W}\boldsymbol{\eta} - {}^{W}\boldsymbol{\eta}^{*} \right\| \tag{38}$$

where, ${}^{W}\boldsymbol{\eta}$ denotes coordinates of the perpendicular vector to the EE surface. Accordingly, the smaller value of stable index, the more precise tracking performance of stabilizer can be achieved. Alternatively, another index is devoted to smoothness of input signal, which is calculated with

$$J_{\text{smooth}} = \|\ddot{\boldsymbol{u}}\| . \tag{39}$$

The smoothness index plays a vital role in the implementation of various algorithms, which impose critical damages to the system actuators due to highly amounts of the smoothness

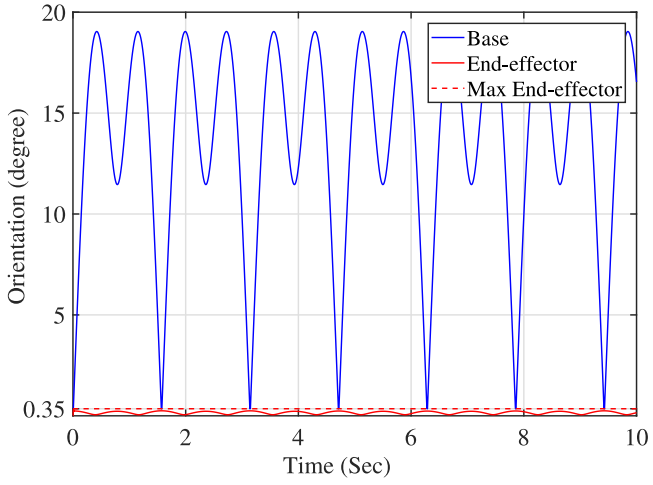

Fig. 6. The simulation results of the proposed method: Demonstrating the EE orientation and base of the 2-DOF SPR.

index. Such algorithms lose their performance in the realistic implementation. As a result, the smoothness index should be taken into account for determining the design parameters.

In Table 1, a realization procedure for evaluating the relation between the design parameters of robust adaptive algorithm and the L_2-norm of indices has been conducted whose results are reported in Fig. 5. It is necessary to mention that in order to provide a consistent measurement for the above defined indices, and due to different number of data samples in simulation and practical studies, in calculation of L_2-norm the square sum of samples is divided to the number of samples. The goal consists in finding optimal values of controller design parameters, η_q and α_q. For each design parameters, a wide range of values is chosen to demonstrate the possible options: slightly small, fairly appropriate, and large values while another parameter is fixed to a specific value. For simplicity, the values of design parameter of output channels are chosen equally. By running several

Table 1
Procedure for tuning the controller design parameters.

Stage	Description	The equivalent in the research
1	Select an appropriate initial guess for η_q and an initial log span for α_q	$\eta_q = 100$, $\alpha_q^0 = [10^{-4}, 10^{-1}]$
2	From the view of both indices, find a suitable span for α_q	$\alpha_q \in [0.001, 0.1]$
3	Select a value from the span for α_q	$\alpha_q = 0.01$
4	Select an initial log span for α_q	$\alpha_q = 0.01$, $\eta_q^0 = [1, 1000]$
5	From the view of both indices, find a suitable span for η_q	$\eta_q \in [1, 1000]$
6	Select a value from the span for η_q	$\eta_q = 300$

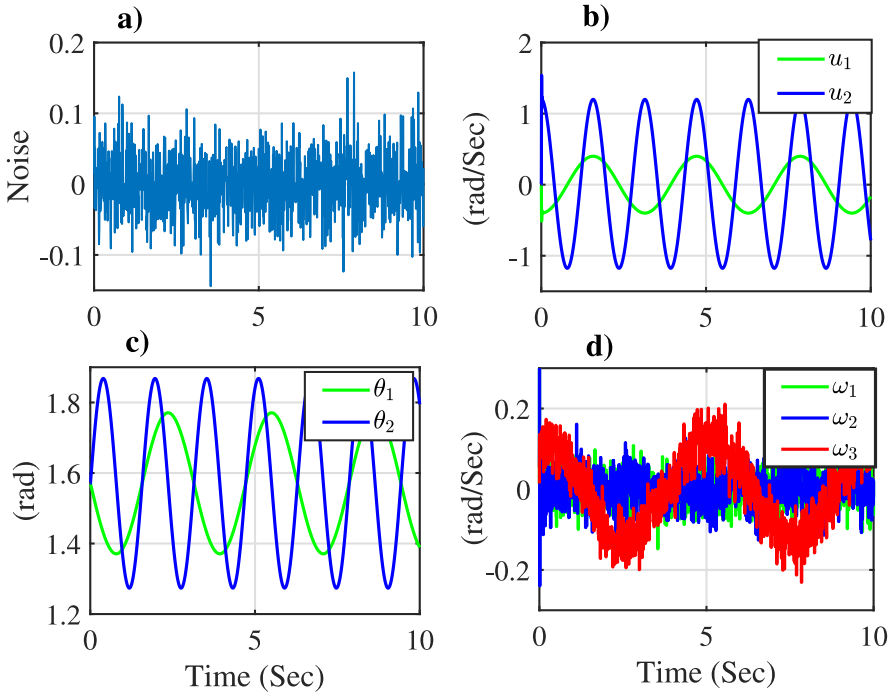

Fig. 7. The simulation results of the proposed method: (a) additive noise in the (d) end-effector angular velocities, (b) the robot input signals, (c) the position of encoders.

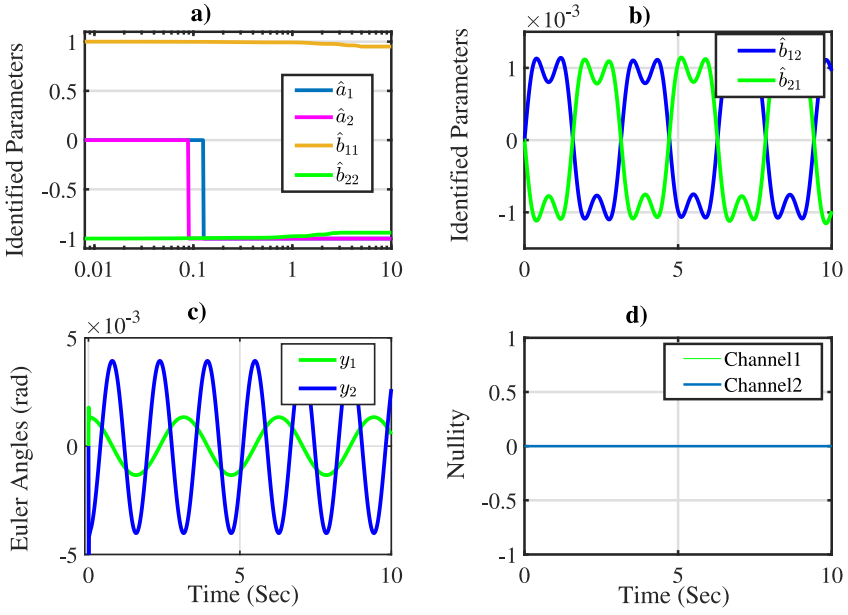

Fig. 8. The simulation results of the proposed method: (a), (b) the identified system parameters, (c) the end-effector Euler angles, (d) nullity of channels.

simulations, the effect of decreasing or increasing the value of design parameters on the indices is demonstrated and evaluated by inspection. To achieve an appropriate stabilization from the view point of L_2-norm of both J_{stable} and J_{smooth}, the parameter

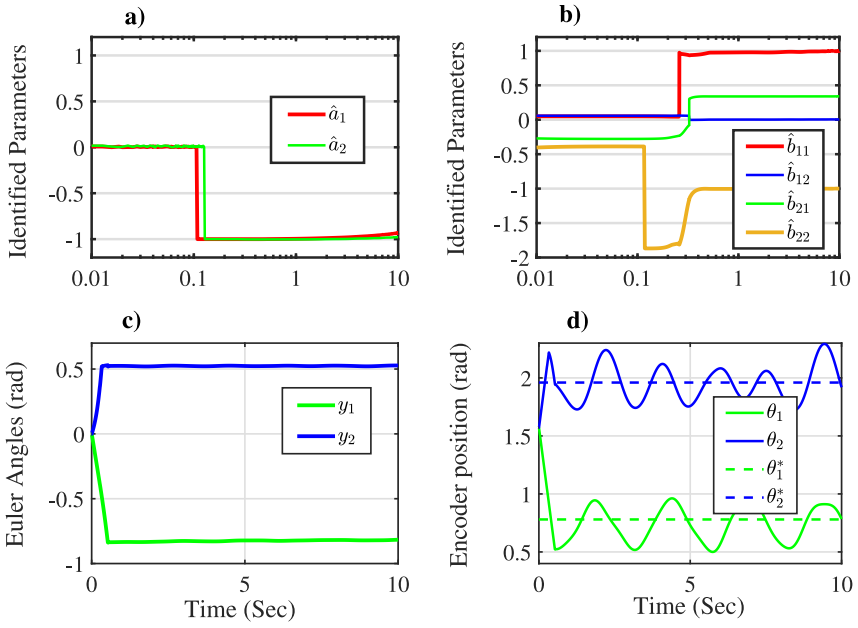

Fig. 9. The simulation results of the proposed method in the stabilization mode: (a), (b) the identified system parameters, (c) the end-effector Euler angles, (d) the position of Encoders.

η_q at each channel should be selected in the range of $[50, 500]$. Moreover, it is demonstrated that the optimal value of α_q at each channel lies in the span $[0.001, 0.1]$ observed by inspection. In the realization procedure, it is noticeable that the effect of design parameters on both indices represents a log function rather than a linear one. Therefore, in spite of choosing linear span, in order to show the effect of small or large amounts of design parameters, a log span of samples is selected for both design parameters. By setting $\eta_q = 300$ and $\alpha_q = 0.01$ from the mentioned spans of design parameters, both indices are satisfied through this paper. Moreover, $\zeta_q = 1, \beta_q = 1.2$ are selected in both simulation and practical experiments.

Thereafter, simulation results of applying the algorithm proposed in Procedure 1 are discussed. In Fig. 6, it is demonstrated that the robust adaptive scheme succeeds to stabilize the EE. The orientation of EE is bounded to 0.35° in existence of considerable excitations, which are applied to the base of EE and formulated in Eq. (37). Moreover, Figs. 7 and 8 show other details of the simulation in which additive noise exists in the EE velocities toward the world frame, and such random values put the stabilizer in much more difficult situations. The input signals, encoder positions, and the EE Euler angles described in the world frame are smoothly obtained, as well. In Fig. 8, the identified parameters of the transfer function, defined in Eq. (5), are plotted during the simulation. Due to highly excited signals applied to the base of the robot, sufficient excitation condition Remark 1 is satisfied for Theorem 1. As a consequence, both nullity of channels, indicated with n_q, remain zero in the simulation procedure. In addition, the identified parameters of matrix $\mathbf{B}$ are acquired diagonally dominant, consequently satisfying the condition of Assumption I.

In order to verify the order-reduced Jacobian matrix, described in Eq. (35), the desired stabilization target is studied in a distinct simulation. In this regard, the output signals are chosen to be stabilized at $\boldsymbol{y}_r(t) = \left(-\frac{\pi}{4}, \frac{\pi}{6}\right)^\top$, and Fig. 9 shows the corresponding results. In the following, the amplitude of base excitation signals are set to $a_x = 0.34$ (rad), $a_y = 0.21$ (rad), and $a_z = 0.12$ (rad), and the corresponding frequencies are also set to $f_x = 3.5$ (rad/s), $f_y = 2.5$ (rad/s), and $f_z = 1.83$ (rad/s). It is demonstrated that the output signals successfully track the desired values, stabilizing the EE at $\left(-\frac{\pi}{4}, \frac{\pi}{6}\right)$. Moreover, $\theta_q, q = 1, 2$ indicates the required variations of Encoder position for stabilizing at the mentioned state. $\theta_q^*, q = 1, 2$, shows the point that the order-reduced Jacobian matrix is calculated in Eq. (36). The identified parameters of the order-reduced Jacobian matrix are acquired from Fig. 9, constructing the elements of $\hat{\boldsymbol{J}}_{\text{red}}$. To assess the identification accuracy of stabilization method, the following relative identification error is employed:

$$\delta_J = \frac{\|\boldsymbol{J}_{\text{red}}(0.78, 1.96) - \hat{\boldsymbol{J}}_{\text{red}}\|}{\|\boldsymbol{J}_{\text{red}}(0.78, 1.96)\|} = 0.0207. \tag{40}$$

where, the obtained value for δ_J demonstrates the relatively small error of identification procedure. Therefore, the proposed method stabilizes the EE at the desired values.

Table 2
Simulation results: Comparing the mentioned methods from the index L_2-norm point of view.

Indices	Proposed	Adaptive	Decay
$\|J_{\text{smooth}}\|_{L_2}$ (rad/s^2)	0.0473	151.3711	334.2205
$\|J_{\text{stable}}\|_{L_2}$ (rad)	4.8639E−5	7.5117E−5	2.2229E−4

Providing appropriate perspective for comparison, two well-known methods are quite completely analyzed in this paper, both of them were previously implemented on the 2-DOF SPR. The decay exponentially algorithm, proposed by Danaei et al. [10], is basically a proportional controller, which has been exploited in a novel way for stabilization purpose. Such a robust method, as a representation for PID controllers, is included in the comparison results. Furthermore, an adaptive approach has been introduced by Ansari et al. [21], mainly in order to conform to the varying environment, and revealed remarkable performance in stabilization of the under study 2-DOF robot. In Fig. 4, the block diagram of PID and adaptive structures are depicted, demonstrating a noteworthy distinguishing feature between such algorithms and the proposed robust adaptive structure. Identifying recursively the Jacobian matrix of the 2-DOF robot, the robust adaptive method stabilizes the EE without requirement of adopting the encoder information. Such a novel advantage makes the proposed method agile and quite more adaptable than other methods.

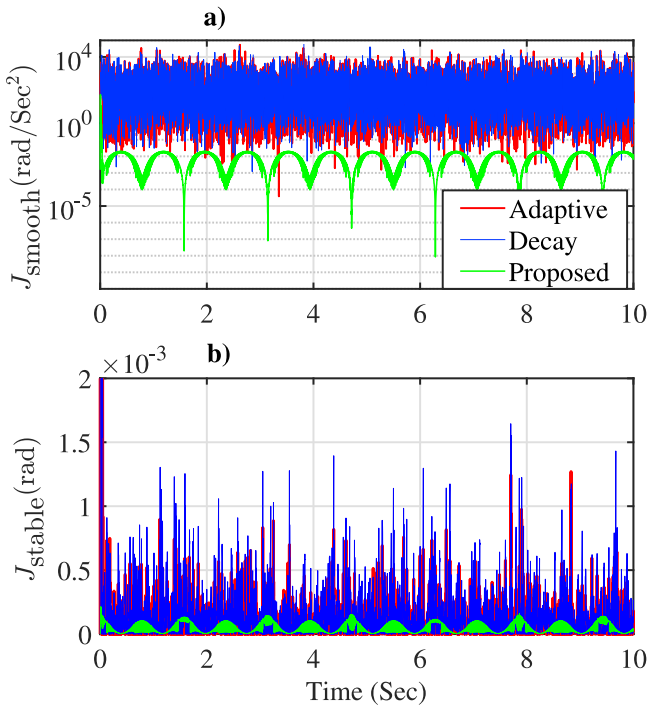

Fig. 10. Simulation results: Comparing (a) J_{smooth} and (b) J_{stable} between the adaptive, Decay, and the proposed method. (For interpretation of the references to color in this figure legend, the reader is referred to the web version of this article.)

Intended to show the superiority of the proposed algorithm, the mentioned methods are simulated in similar conditions. The parameters of adaptive controller are chosen as $\gamma = 10^4$, $k_{adaptive} = 300$ and the gain of decay exponentially algorithm is set to $k_{decay} = 200$, as well. In Fig. 10, the result of simulations are demonstrated, where the indices are plotted for each method. From stability point of view, J_{stable} indicates that the proposed robust adaptive scheme leads to a remarkable performance. Despite severe external excitations, the stability index (the green lines) remains bounded under 5×10^{-4} (rad), while the other two algorithms cross 5×10^{-4} (rad) several times during the simulation procedure. As aforementioned, the smoothness index indicates the performance of algorithms when it comes to practical implementation. Although, it is demonstrated that both adaptive and decay exponentially approaches impose relatively considerable variations to the input signals, the proposed robust adaptive approach limits such variations, leading to a smooth algorithm for stabilization of parallel robots. Table 2 compares the methods from the L_2-norm of indices. Despite Fig. 10, where peaks of indices are of importance, in Table 2 the norm of the indices is adopted as a criterion, where J_{smooth} and J_{stable} are acquired as 0.047 (rad/s^2) and 4.86×10^{-5} (rad), respectively. As a result, one can infer that the robust adaptive scheme reveals better performance in comparison with the other algorithms.

4.2. Path tracking

In this part, tracking a desired path, as another feature of the proposed structure, is simulated. In the following simulation, no external excitations is applied to the base of the robot, creating the opportunity to simply analyze the tracking ability. In this regard, the desired path is $y_{r_1} = \frac{\pi}{6}\sin(4t)$ (rad), $y_{r_2} = \frac{\pi}{6}\cos(4t)$ (rad). Fig. 11 shows the tracking results in which the output signals precisely track the desired values. Nonetheless, the identified parameters do not converge to any specific values from the Jacobian matrix point of view, Eq. (36). The observation makes sense according to the varying stabilization state at each moment. In another word, since θ_q^* is dependent on time, Eq. (36) is not established, leading to an unreliable identified parameters.

5. Practical implementation

In this section, the proposed approach is implemented on the 2-DOF SPR and the practical implementation results are available in Appendix A. Setup components are shown in Fig. 12. Two Dynamixel Mx-64AR motors are employed as actuator because of their high accuracy and ability of control in both position and

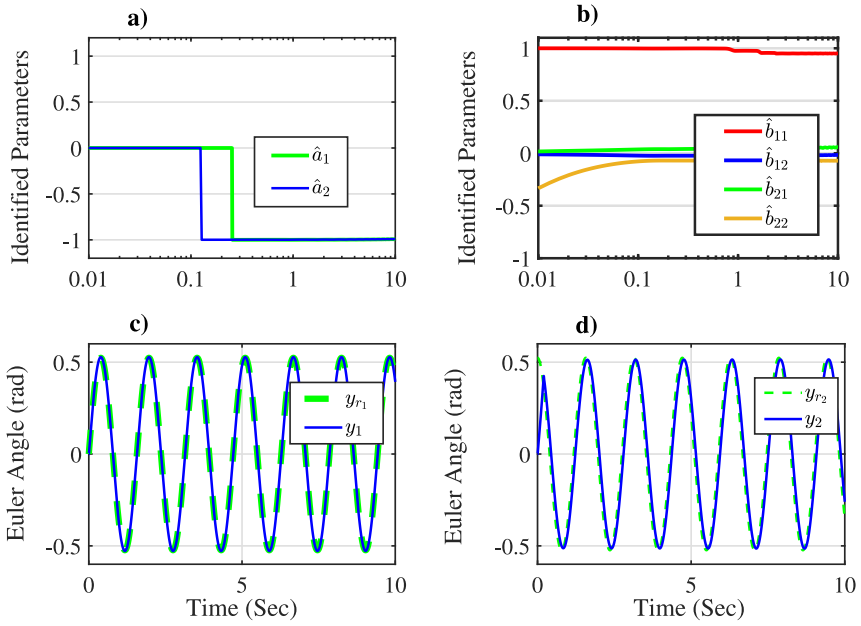

Fig. 11. The simulation results of the proposed method in the tracking mode: (a), (b) the identified system parameters, (c), (d) the desired paths for the end-effector Euler angles.

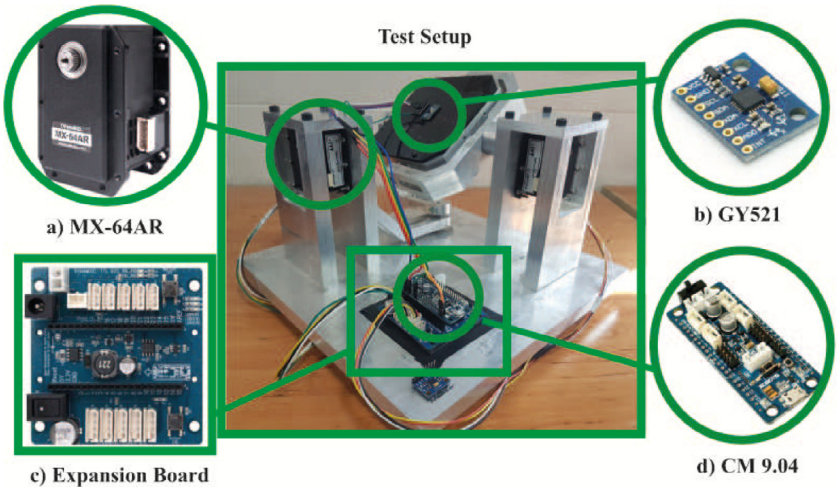

Fig. 12. Test setup of the 2-DOF SPR.

Table 3
Practical results: Comparing the mentioned methods from the index L_2-norm point of view.

Indices	Proposed	Adaptive	Decay
$\|J_{\text{smooth}}\|_{L_2}$ (rad/s^2)	2.677	3.513	5.685
$\|J_{\text{stable}}\|_{L_2}$ (rad)	0.026	0.042	0.096
$\|J_{\text{damp}}\|_{L_2}$	0.091	0.136	0.278

velocity mode. A Gy521 module is mounted on the EE to measure angular velocity and Euler angles. There are two sensors in the module: 3-axial accelerometer and 3-axial gyroscope sensor. Moreover, the module possess a high performance digital motion processor, proving the ability to handle complicated algorithms. Intended to connect the module to the main circuit, I2C protocol is utilized. To process information that is obtained through the Gy521, Opencm9.04 is employed as a main processor which is connected to actuators with an expansion board, namely OpenCM 485 EXP. In order to program Opencm9.04, Arduino IDE is utilized instead of OpenCM by adopting Dynamixel Workbench library. In the practical experiments, $\eta_q = 100$ and $\alpha_q = 0.01$, $\zeta_q = 1$, $\beta_q = 1.2$ are set in order to achieve acceptable performance in tracking as well as reducing the identification error.

The main challenges in obtaining the research results are devoted to both theoretical and practical parts. Firstly, imposing and surveying different realistic conditions, specially having bounded disturbances in each output channel, for the designed controller, different theories are written intended to show the systematic guarantee that the aforementioned control approach requires to be validated. Secondly, the practical implementation faces several challenges, to name but a few, finding suitable and reliable actuators, reading data from Gyro sensors and programming them, coping with existing noises while reading data and sending commands to the actuators, implementation of a fast version of the controller algorithm, and finding optimal values of the design controller parameters as for the 2-DOF parallel robot.

5.1. Stabilization

In order to compare performance of proposed method with decay exponentially algorithm and adaptive approach, practical results of the mentioned methods are studied. Fig. 13 contains the orientation of EE and the base, also shows the performance of the exponentially decay algorithm and adaptive approach, respectively. It is vital to note that external excitations are applied to the base of robot by hand movement. Proposed method succeeds to

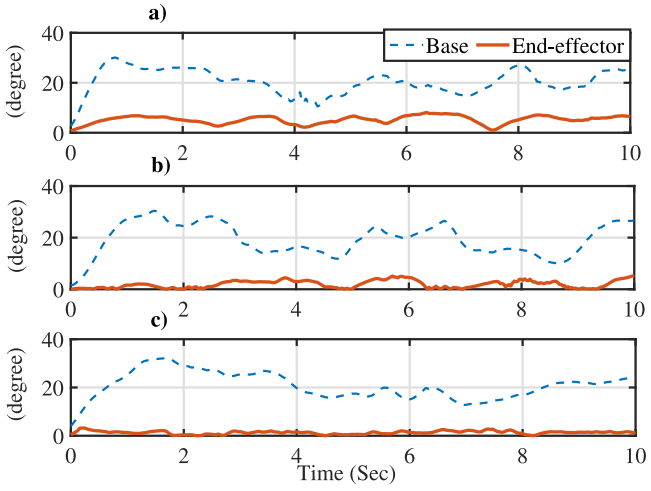

Fig. 13. Practical results: Comparing the orientation of the base and the end-effector between the (a) Decay, (b) adaptive, and (c) the proposed methods.

stabilize the base excitations. In addition, the approach reveals better performance in comparison with the other two method in disturbance rejection. Table 3 compares the methods from the perspective of L_2 norm of indices. In this part, in addition to the two previous indices that were introduced in Section 4, a new index has been utilized:

$$J_{\text{damp}} = \text{orientation}_{\text{EE}}/\text{orientation}_{\text{Base}}. \tag{41}$$

This index illustrates that how much each method has been successful in reducing the disturbance. In this regard, J_{smooth} and J_{stable} are acquired as 2.67 (rad/s^2) and 0.026 (rad), respectively. Moreover, the damp ratio is obtained as 0.091 which demonstrates the superiority of the robust adaptive scheme in comparison with other algorithms. These results verify outcomes that have been obtained in the simulation.

It is worth noting that by surveying the different scenarios of the proposed robust adaptive approach, having insufficient excitation signals as the reference tracking path is handled in Procedure 1. Nonetheless, it has been demonstrated that in both Sections 4.1 and 5.1, it is not required to apply the provided insufficient excitation handler even though the signals are steady, considered as insufficient excitation signals. In this regard, the 2-DOF SPR provides agile movements so that it maintains

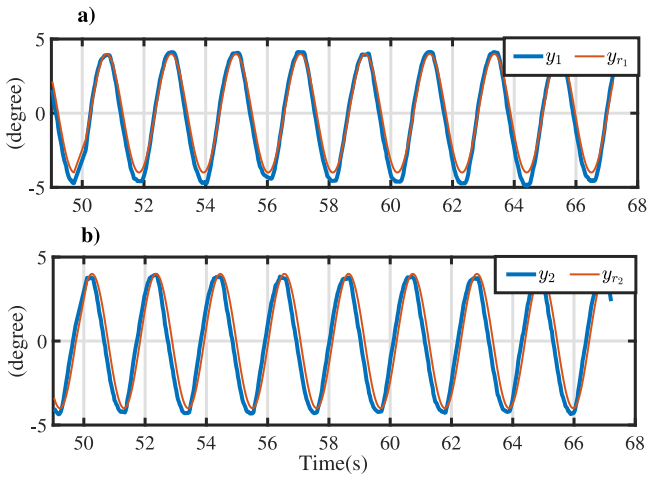

Fig. 14. The end-effector Euler angles and the corresponding desired values.

the condition number of Covariance matrices of data limited. Therefore, in both stabilization of simulation and practical cases, non-persistent excitation signals have been already applied and the proposed robust adaptive method handles smoothly. In [56], it has been demonstrated that the proposed robust adaptive method, implemented on a 3-DOF SPR, faces with insufficient excitation signals. Consequently, a novel SVD-based method is suggested which has been implemented on the 3-DOF SPR for handling insufficient excitation signals with rank deficiency at each channel.

5.2. Path tracking

In this part, the ability of the proposed method in path tracking is studied. In the following implementation, the same as path tracking in simulation, base excitations have not been considered. In this case, the desired path is $y_{r_1} = 4\sin(3t)$ and $y_{r_2} = 4\cos(3t)$. The tracking results are shown in Fig. 14 in which the output signals accurately track the desired path and verify the outcomes obtained in Section 5.2. Predicated on Theorem 1, the proposed method is able to attenuate the model uncertainties appeared in each channel. By setting appropriate design parameters, the error of output tracking and identification vanishes. As a result, this proposed method guarantees that by having an unbiased noise in the output channel, the system tracks the desired output signals and identifies the parameters completely. Moreover, having colored noise in the output channels, the proposed method handles the effect of the drift with the least possible error in both control and identification tasks.

6. Conclusion

In this paper, a novel robust adaptive scheme was proposed which guarantees the simultaneous identification and control of a system in the presence of bounded disturbances, intended to conform to the surrounding environments and cope with uncertainties during control procedure. Thereafter, based on the introduced robust adaptive controller, a novel approach was presented in order to control the MIMO system outputs, i.e., the EE Euler angles of 2-DOF spherical parallel robot, with handling the insufficient excitation at each output channel and without any prior knowledge about the Jacobian Matrix, Inverse, or Forward Kinematic equations of the robot. It manipulates the system inputs in order to stabilize the end-effector of 2-DOF robot, by identifying unknown system parameters, having being shown that comprise the Jacobian matrix elements. The proposed approach of the paper was compared with that of two well-known methods: an adaptive method in which parameters conform to the uncertainties and an exponentially decay algorithm, which chooses a proportional gain to stabilize the robot. In this regard, the proposed approach possesses a distinct advantages over mentioned methods, that is, not involving the information of encoders in the control procedure, leads to having much higher sampling rate. Moreover, the suggested method imposes signals with the least possible variations to the actuators, and reveals remarkable performance in damping the external excitations applied to the based. The norm of damp index which measures the ratio of EE orientation to the base orientation was acquired as 0.091, demonstrating favorable stabilization in comparison with that of other two methods in both simulation study and implementation stage. In the simulation analysis, it was demonstrated that the robust adaptive scheme tries to estimate the Jacobian matrix in order to acquire an adaptation to the robot states. Accordingly, the relative identification error of Jacobian matrix was obtained as 0.0207 in the stabilization mode. The proposed structure also revealed a precise performance in tracking desired paths for the EE Euler angles. As an ongoing study, the idea of combination of the proposed scheme with a reinforcement algorithm seems as a cutting-edge notion in order to optimize the control effort during the identification procedure.

Declaration of competing interest

The authors declare that they have no known competing financial interests or personal relationships that could have appeared to influence the work reported in this paper.

Appendix A. Practical implementation results

Supplementary material related to this article can be found online at https://doi.org/10.1016/j.isatra.2021.02.001.

References

[1] Chen S, Li Y, Kwok NM. Active vision in robotic systems: A survey of recent developments. Int J Robot Res 2011;30(11):1343–77.
[2] Hilkert J. Inertially stabilized platform technology concepts and principles. IEEE Control Syst Mag 2008;28(1):26–46.
[3] Řezáč M, Hurák Z. Structured MIMO h design for dual-stage inertial stabilization: Case study for HIFOO and hinfstruct solvers. Mechatronics 2013;23(8):1084–93.
[4] Egbert J, Beard RW. Low-altitude road following using strap-down cameras on miniature air vehicles. Mechatronics 2011;21(5):831–43.
[5] Sachs D, Nasiri S, Goehl D. Image stabilization technology overview. InvenSense whitepaper, 2006.
[6] Amanatiadis A, Gasteratos A, Papadakis S, Kaburlasos V. Image stabilization in active robot vision. INTECH Open Access Publisher; 2010.
[7] Qiang Y, Baifeng W, Yi J, Kun Z. Summarization of electronic image stabilization. In: 2006 7th international conference on computer-aided industrial design and conceptual design. IEEE; 2006, p. 1–5.
[8] Van Lanh T, Chong K-S, Emmanuel S, Kankanhalli MS. A survey on digital camera image forensic methods. In: 2007 IEEE international conference on multimedia and expo. IEEE; 2007, p. 16–9.
[9] Hesar ME, Masouleh M, Kalhor A, Menhaj M, Kashi N. Ball tracking with a 2-DOF spherical parallel robot based on visual servoing controllers. In: 2014 second RSI/ISM international conference on robotics and mechatronics. IEEE; 2014, p. 292–7.
[10] Danaei B, Alipour M, Arian A, Masouleh MT, Kalhor A. Control of a two degree-of-freedom parallel robot as a stabilization platform. In: 2017 5th RSI international conference on robotics and mechatronics. IEEE; 2017, p. 232–8.
[11] Bozorgi ERJ, Yahyapour I, Karimi A, Masouleh MT, Yazdani M. Design, development, dynamic analysis and control of a 2-DOF spherical parallel mechanism. In: 2014 second RSI/ISM international conference on robotics and mechatronics. IEEE; 2014, p. 445–50.

[12] Safaryazdi A, Zarei M, Abolghasemi O, Tale Masouleh M. Experimental study on the model-based control of a 2-degree-of-freedom spherical parallel robot camera stabilizer based on multi-thread programming concept. Proc Inst Mech Eng C 2018;232(10):1882–97.
[13] Kennedy PJ, Kennedy RL. Direct versus indirect line of sight (LOS) stabilization. IEEE Trans Control Syst Technol 2003;11(1):3–15.
[14] Seong K-J, Kang H-G, Yeo B-Y, Lee H-P. The stabilization loop design for a two-axis gimbal system using LQG/LTR controller. In: 2006 SICE-ICASE international joint conference. IEEE; 2006, p. 755–9.
[15] Roshdy AA, Lin YZ, Su C, Mokbel HF, Wang T. Design and performance of non-linear fuzzy logic PI controller for line of sight stabilized platform. In: 2012 international conference on optoelectronics and microelectronics. IEEE; 2012, p. 359–63.
[16] Zakia U, Moallem M, Menon C. PID-SMC controller for a 2-DOF planar robot. In: 2019 international conference on electrical, computer and communication engineering. IEEE; 2019, p. 1–5.
[17] Sahu UK, Mishra A, Sahu B, Pradhan PP, Patra D, Subudhi B. Vision-based tip position control of a 2-DOF single-link robot manipulator. In: Proceedings of international conference on sustainable computing in science, technology and management. IEEE; 2019, p. 1–7.
[18] Van M, Do XP, Mavrovouniotis M. Self-tuning fuzzy PID-nonsingular fast terminal sliding mode control for robust fault tolerant control of robot manipulators. ISA Trans 2019;1:1–12.
[19] Guo Q, Yu T, Jiang D. Robust H positional control of 2-DOF robotic arm driven by electro-hydraulic servo system. ISA Trans 2015;59:55–64.
[20] Yin X, Pan L. Direct adaptive robust tracking control for 6 DOF industrial robot with enhanced accuracy. ISA Trans 2018;72:178–84.
[21] Ansari-Rad S, Zarei M, Ghafarian Tamizi M, Mohammadi Nejati S, Tale Masouleh M, Kalhor A. Stabilization of a two-DOF spherical parallel robot via a novel adaptive approach. In: 2018 6th RSI international conference on robotics and mechatronics. IEEE; 2018, p. 369–74.
[22] Arian A, Danaei B, Masouleh MT. Kinematics and dynamics analysis of a 2-DOF spherical parallel robot. In: 2016 4th international conference on robotics and mechatronics. IEEE; 2016, p. 154–9.
[23] Yue F, Li X. Robust adaptive integral backstepping control for opto-electronic tracking system based on modified LuGre friction model. ISA Trans 2018;80:312–21.
[24] Li Q, Yuan J, Zhang B, Wang H. Artificial potential field based robust adaptive control for spacecraft rendezvous and docking under motion constraint. ISA Trans 2019;1:1–12.
[25] Peng J, Yang Z, Wang Y, Zhang F, Liu Y. Robust adaptive motion/force control scheme for crawler-type mobile manipulator with nonholonomic constraint based on sliding mode control approach. ISA Trans 2019;1:1–12.
[26] Hashemi M, Shahgholian G. Distributed robust adaptive control of high order nonlinear multi agent systems. ISA Trans 2018;74:14–27.
[27] Zhu Z-C, Li X, Shen G, Zhu W-D. Wire rope tension control of hoisting systems using a robust nonlinear adaptive backstepping control scheme. ISA Trans 2018;72:256–72.
[28] Ansari-Rad S, Hashemi M, Salarieh H. Pseudo DVL reconstruction by an evolutionary TS-fuzzy algorithm for ocean vehicles. Measurement 2019;1:1–12.
[29] Ansari-Rad S, Kalhor A, Araabi BN. Partial identification and control of MIMO systems via switching linear reduced-order models under weak stimulations. Evol Syst 2019;10(2):111–28.
[30] Tsai JS-H, Du Y-Y, Huang P-H, Guo S-M, Shieh L-S, Chen Y. Iterative learning-based decentralized adaptive tracker for large-scale systems: A digital redesign approach. ISA Trans 2011;50(3):344–56.
[31] Radac M-B, Precup R-E, Roman R-C. Data-driven model reference control of MIMO vertical tank systems with model-free VRFT and Q-learning. ISA Trans 2018;73:227–38.
[32] Xu Y, Zhou W, Fang J, Sun W. Adaptive lag synchronization and parameters adaptive lag identification of chaotic systems. Phys Lett A 2010;374(34):3441–6.
[33] Jahandari S, Kalhor A, Araabi BN. Online forecasting of synchronous time series based on evolving linear models. IEEE Trans Syst Man Cybern A 2018;1(99):1–12.
[34] Lee C-H, Teng C-C. Identification and control of dynamic systems using recurrent fuzzy neural networks. IEEE Trans Fuzzy Syst 2000;8(4):349–66.
[35] Ren X, Rad AB, Chan P, Lo WL. Identification and control of continuous-time nonlinear systems via dynamic neural networks. IEEE Trans Ind Electron 2003;50(3):478–86.
[36] Chen M, Ge SS, Ren B. Adaptive tracking control of uncertain MIMO nonlinear systems with input constraints. Automatica 2011;47(3):452–65.
[37] Dass A, Srivastava S. Identification and control of dynamical systems using different architectures of recurrent fuzzy system. ISA Trans 2019;85:107–18.
[38] Feng H, Yin C, Ma W, Yu H, Cao D. Parameters identification and trajectory control for a hydraulic system. ISA Trans 2019;1:1–12.
[39] Lee JY, Park JB, Choi YH. Integral q-learning and explorized policy iteration for adaptive optimal control of continuous-time linear systems. Automatica 2012;48(11):2850–9.
[40] Jiang Y, Jiang Z-P. Computational adaptive optimal control for continuous-time linear systems with completely unknown dynamics. Automatica 2012;48(10):2699–704.
[41] Modares H, Lewis FL. Linear quadratic tracking control of partially-unknown continuous-time systems using reinforcement learning. IEEE Trans Automat Control 2014;59(11):3051–6.
[42] Chen C, Modares H, Xie K, Lewis FL, Wan Y, Xie S. Reinforcement learning-based adaptive optimal exponential tracking control of linear systems with unknown dynamics. IEEE Trans Automat Control 2019;1:1–12.
[43] Jia C, Li X, Wang K, Ding D. Adaptive control of nonlinear system using online error minimum neural networks. ISA Trans 2016;65:125–32.
[44] Izadbakhsh A, Khorashadizadeh S, Ghandali S. Robust adaptive impedance control of robot manipulators using Szász–Mirakyan operator as universal approximator. ISA Trans 2020.
[45] Yang S, Han J, Xia L, Chen Y-H. An optimal fuzzy-theoretic setting of adaptive robust control design for a lower limb exoskeleton robot system. Mech Syst Signal Process 2020;141:106706.
[46] Yang S, Han J, Xia L, Chen Y-H. Adaptive robust servo constraint tracking control for an underactuated quadrotor UAV with mismatched uncertainties. ISA Trans 2020.
[47] Yin X, Zhang W, Jiang Z, Pan L. Adaptive robust integral sliding mode pitch angle control of an electro-hydraulic servo pitch system for wind turbine. Mech Syst Signal Process 2019;133:105704.
[48] Hernández JH, Cruz SS, López-Gutiérrez R, González-Mendoza A, Lozano R. Robust nonsingular fast terminal sliding-mode control for sit-to-stand task using a mobile lower limb exoskeleton. Control Eng Pract 2020;101:104496.
[49] Gosselin C, Angeles J. Singularity analysis of closed-loop kinematic chains. IEEE Trans Robot Autom 1990;6(3):281–90.
[50] Danaei B, Arian A, Masouleh MT, Kalhor A. Dynamic modeling and base inertial parameters determination of a 2-DOF spherical parallel mechanism. Multibody Syst Dyn 2017;41(4):367–90.
[51] Ansari-Rad S, Jahandari S, Kalhor A, Araabi BN. Identification and control of MIMO linear systems under sufficient and insufficient excitation. In: 2018 annual American control conference. IEEE; 2018, p. 1108–13.
[52] Åström KJ, Wittenmark B. Adaptive control. Courier Corporation; 2013.
[53] Briot S, Bonev IA. Pantopteron: A new fully decoupled 3DOF translational parallel robot for pick-and-place applications. J Mech Robot 2009;1(2):021001.
[54] Li W, Zhang J, Gao F. P-cube, a decoupled parallel robot only with prismatic pairs. In: 2006 2nd IEEE/ASME international conference on mechatronics and embedded systems and applications. IEEE; 2006, p. 1–4.
[55] Yahyapour I, Hasanvand M, Masouleh MT, Yazdani M, Tavakoli S. On the inverse dynamic problem of a 3-PRRR parallel manipulator, the tripteron. In: 2013 first RSI/ISM international conference on robotics and mechatronics. IEEE; 2013, p. 390–5.
[56] Rad SA, Tamizi MG, Azmoun M, Masouleh MT, Kalhor A. Experimental study on robust adaptive control with insufficient excitation of a 3-DOF spherical parallel robot for stabilization purposes. Mech Mach Theory 2020;153:104026.